ICAS 2020 SHANGHAI
International Council of the Aeronautical Sciences
32nd Congress of the International Council of the Aeronautical Sciences
September 6-10, 2021
Pudong Shangri-La, Shanghai, China

# Design and Test of a High Slope Angle Intermediate Duct between Low-Pressure Compressor and High-Pressure Compressor

Hailiang JIN, Jun ZHANG, Junfeng WU, Daobin QIU & Yueqian YIN

AECC Hunan Aviation Powerplant Research Institute, Hunan Key Laboratory of Turbomachinery on Small and Medium Aero-Engine, Zhuzhou, China, 412002

## Abstract

Flow path and strut airfoil aerodynamic design were completed for a high slope angle intermediate duct between low-pressure compressor (LPC) and high-pressure compressor (HPC). Three dimensional CFD computations were used to simulate the flow field of the intermediate duct. Flow test rig design, instrumentation and flow test were conducted to obtain the performance of the intermediate duct. The CFD results show that the average flow accelerates slightly from the inlet to the outlet of the intermediate duct. The flow along the hub firstly accelerates and then decelerates whereas the flow along the shroud firstly accelerates then keeps approximately constant velocity. The corner separation between the end-wall and strut surface near trailing edge contributes the main loss in the intermediate duct. The test results indicate that the measured total pressure recovery coefficient of the intermediate duct is 0.3 percent higher than the design goal but 0.3 percent lower than the CFD computation result.

**Keywords:** compressor, slope angle, intermediate duct, strut, flow test, loss

## 1. Introduction

The intermediate duct is an important component connecting the LPC and the HPC in the aero engine. The main function of intermediate duct is to guide the airflow compressed by the LPC into the HPC with lower loss and better flow field quality. The radius difference between the LPC outlet and the HPC inlet is increasing in modern aero engines, whereas the axial length of the intermediate casing is decreasing due to the strict restrictions on weight and rotor dynamics of the aero engine. It will bring more losses when the flow is deflecting from LPC outlet to HPC inlet with a larger radius drop in a short axial length. The upstream fully developed wake and end wall boundary layer will easily induce secondary flow and boundary layer separation in the corner of the end wall and strut, which leads to massive flow losses. Therefore, the intermediate duct design with short axial length and large radius difference between inlet and outlet has always been the goal in high-performance engine design.

Baily [1] [2] et al. studied the flow details in the S-shaped intermediate duct through experiments. Dueñas [3] et al. further studied the effect of the length of the S-shaped annular duct on the performance of the intermediate casing. Zhang Guochen [4] et al. studied the internal flow details of S-shaped twin-branch duct using numerical methods. Liu Bo, Wang Yangang et al. [5] [6] studied the influence of the stagger angle and axial locations of the struts on the upstream flow field.

The design of a high slope angle intermediate duct between LPC and HPC was conducted in this paper. The flow path design of the intermediate duct employs a parametric method, and the struts are designed through 3D approaches. Three dimensional CFD computations were performed to obtain the performance and flow field of the intermediate duct. CFD results show that the performance of the intermediate duct can satisfy the design requirements. Finally, the annular cascade flow test rig of the intermediate duct was designed to complete the performance test. The test results of the intermediate duct loss characteristics and outlet flow field are analyzed and compared with the CFD results. The method and results in this paper can provide a valuable reference for a similar intermediate duct design.

## 2. Design Requirements

The main parameters of the intermediate duct studied in this paper are shown in Table 1. The intermediate duct is located between the LPC and HPC. The axial length of the intermediate duct is 118mm, the inlet Mach number is 0.4, and the mean-line slope angle from inlet to outlet is 24°.

Table 1 - Main parameters of the intermediate duct

| Parameters | Values |
|---|---|
| Inlet flow angle (°) | 0 |
| Inlet Mach number | 0.4 |
| Total pressure recovery coefficient (design goal) | 0.985 |

## 3. Design and Analysis of the Intermediate Duct

The flow path design of intermediate duct is conducted by using numerical optimization method based on parametric curves and CFD computations. The contour lines of hub and shroud are determined by a 5$^{th}$-order Bezier curve. Parameterization of the intermediate duct and strut geometry is shown in Fig. 1. The mean-line of this duct features a s-shape, and the flow passage area increases at first and then decreases alone the stream-wise direction. It is necessary to take into account the velocity distribution along hub and tip end-walls when designing their contour lines. The velocity along a streamline should be made as uniform as possible, the velocity difference between hub and tip sections at the outlet of the intermediate duct should also be reduced as much as possible, to eliminate the inlet distortion of HPC.

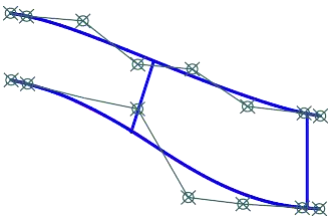

Figure 1 – Parametric representation of the intermediate duct and strut geometry.

The ANSYS CFX software was used to perform the three-dimensional steady-state viscous computation of the intermediate duct. The k-e turbulence model was selected, and the total temperature (288.15K) and total pressure (101325Pa) were specified at the inlet, and an average static pressure was imposed at the outlet. Figure 2 shows the shape of the intermediate duct and strut.

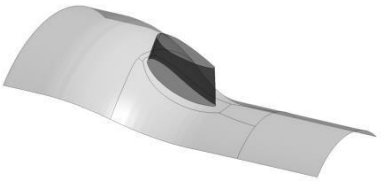

Figure 2 – The intermediate duct and strut.

Figure 3 shows the meridional streamlines of the intermediate duct at the design point. From the figure, it can be seen that the flow in the intermediate section is good, and there is no obvious secondary flow and separation. Figure 4 shows the meridional static pressure field in the intermediate section at the design point. It can be seen from the figure that the tip of the intermediate section has a favorable pressure gradient, which is beneficial to mitigate the flow separation, while the hub static pressure distribution is relatively smooth, which can reduce the diffusion loss due to the adverse pressure gradient.

Figure 5 shows the static pressure profiles from inlet to outlet at the hub, mid-span and tip sections of the intermediate duct at near-design point. It can be seen that the static pressure firstly decreases and then increase at the hub section which indicate the flow first acceleration and then deceleration. So the hub curve of the intermediate duct should be carefully adjusted to avoid the flow separation at hub section. The static pressure distribution of tip section is relatively uniform. The total pressure and outlet entropy contours of the intermediate duct at near design point are shown in Fig. 6 and Fig.

7 respectively. The loss of the hub corner formed by the struts and the annular walls are relatively high, which is one of the main loss sources of the intermediate duct.

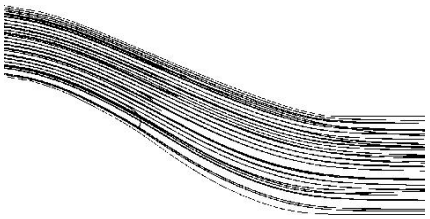

Figure 3 – Meridional streamline at near-design point.

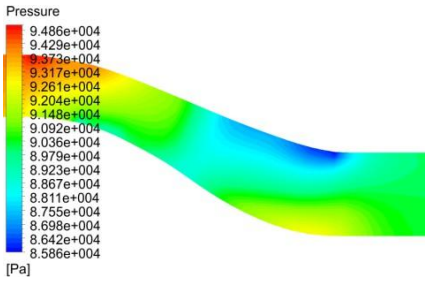


Figure 4 – Meridional static pressure contours at design point.

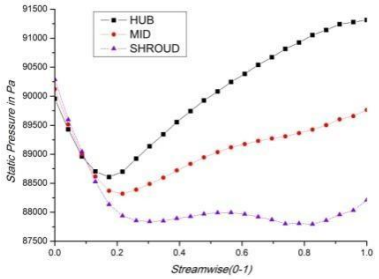


Figure 5 –Static pressure distributions at the hub, mid-span and tip sections at near design point.

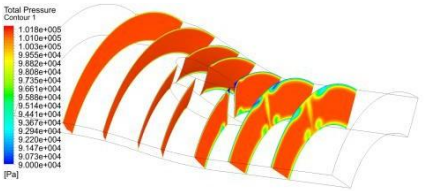


Figure 6 – Total pressure contours on surfaces along the streamwise direction.

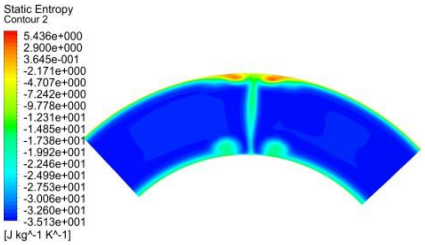


Figure 7 – Static entropy contours at the outlet of the intermediate duct.

## 4. Test Rig Design and Test

Figure 8 displays the general arrangement of the annular cascade test rig, which indicates it is a suction-type rig with a downstream blower. The rig is consisted of the bell mouth, intake cone, intermediate duct body, struts, outer measurement casing, inner measurement casing and exhaust cone. and Fig.9 shows the installation of rig body and instrumentation pipes.

As shown in Fig. 8, the aerodynamic measurement planes are arranged at the inlet and outlet of the intermediate duct, where the axial position of the 1-1 section is located upstream of the front

installation edge of the intermediate duct parts, and the circumferential measurement points are arranged as shown in Fig. 10, respectively. There are 4 static pressure taps, 3 five-point total pressure rakes and 3 five-point total temperature rakes at the inlet measurement plane, all of which are distributed uniformly in the circumferential direction. And the radial positions of pressure and temperature sensors are specially selected they split the flow passage into several parts with the same area.

The axial position of the 2-2 plane is located downstream of the rear mounting edge of the intermediate duct. The circumferential measuring plan is arranged as shown in Fig. 11. They are 12 static pressure taps and 3 five-point total pressure rakes, distributed uniformly in the circumferential direction. And the radial locations of pressure sensors are selected in the same manner as the inlet measurement plane. Moreover, the probes can traverse circumferentially, and therefore a detailed total pressure field can be acquired.

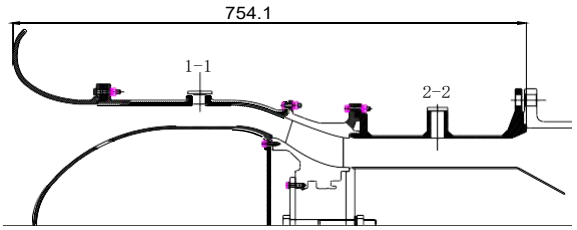

Figure 8 – General arrangement of the annular cascade test rig.


Figure 9 – Installation of the test rig and instrumentation pipes.

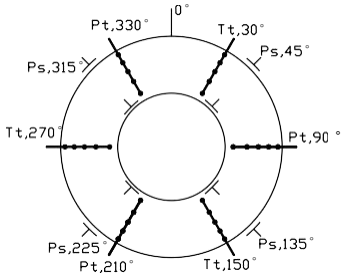

Figure 10 – Instrumentation arrangement for the inlet measurement plane.

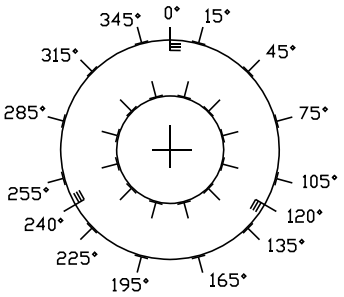

Figure 11 – Instrumentation arrangement for the outlet measurement plane.

The cascade test is conducted at HAPRI's wind tunnel. By adjusting the power of blower, the desired inlet mass flow rate can be achieved. Several operating points are selected to cover the design point and to get a line which represents the performance characteristic.

Figure 12 displays the characteristics lines in terms of total pressure recovery coefficient versus the inlet mass flow rate, which are obtained from cascade experiment and 3D CFD calculation respectively. Although the test shows a lower recovery coefficient than that predicted by CFD calculation in the whole mass flow range, these two sets of data show a very good agreement in trend. And at the near-design point, the figure for experiment result is 0.3% lower, compared to the value provided by numerical computation.

Figure 13 shows the spanwise distribution for the total pressure recovery coefficient of the intermediate duct at near-design point. Both the experiment and CFD computation indicate that there is little pressure loss in region ranging from 30% to 70% span, namely the mainstream. And the data from test and numerical simulation are very close for this mainstream. When the span is under 30% or over 70%, the total pressure recovery coefficient starts to drop dramatically, showing that the pressure recovery is mainly limited by this near end-wall region. The total pressure and entropy contours in Fig. 6 and Fig. 7 suggest that the loss is mainly due to the end-wall boundary layer and corner secondary flow. The development of boundary layer is affected by the surface roughness, and it is not fully simulated in this CFD calculation, which may contribute to part of the differences between the recovery coefficients from experiment and CFD calculation.

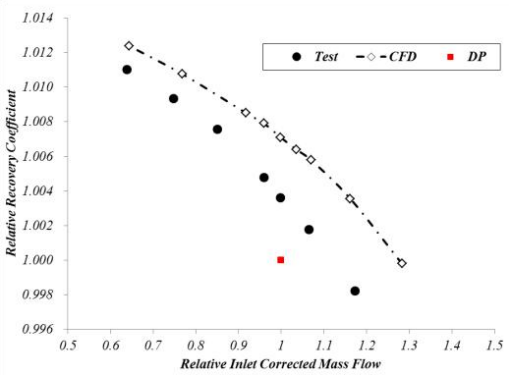


Figure 12 – Total pressure recovery coefficient - inlet mass flow rate characteristic.

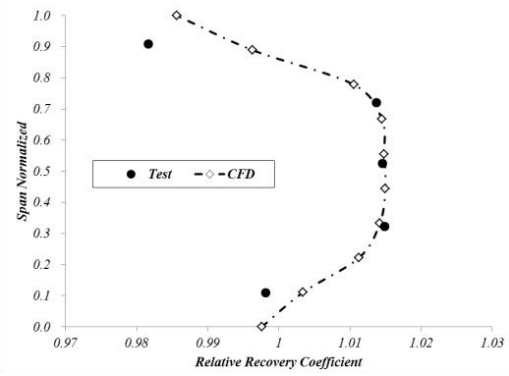


Figure 13 – Spanwise distribution of the total pressure recovery coefficient at near design point.

## 5. Conclusions

A high-slope-angle intermediate duct is designed through optimizing methods to connect the LPC and HPC, aiming at reducing the flow losses, and it is then tested in the wind tunnel to obtain the aerodynamic performance. The specific conclusions obtained are as follows:

(1) The total pressure recovery coefficient of the intermediate duct decreases as the flow rate increases, and the total pressure recovery coefficient at design point is 0.4% higher than the design target according to the test, verifying the performance.

(2) The lower recovery coefficients near hub and tip are mainly due to secondary flow at the corner between the struts and end-walls. Optimization of strut thickness profile and end-wall contouring would be the future development of the intermediate duct.

(3) In the three-dimensional calculation, the influence of surface roughness is not accounted for, leading the CFD calculation to predict a higher recovery coefficient than the cascade test does.

After improving the surface roughness, the total pressure recovery coefficient of the intermediate duct can be further improved.

## 6. Acknowledgement

This paper is supported by the Aviation Science Foundation (2015ZB08006).

## 7. Copyright Statement



## References

[1] Bailey D W. The aero dynamic performance of an annular s-shape duct[D]. UK, Department of Aeronautical and Automotive Engineering and transport studies, Loughborough University, 1997.

[2] Bailey D W, Britchford K M, Carrote J F, et al. Performance assessment of an annular S-shaped duct [J]. Journal of Turbo machinery, 1997, 199(1): 149-156.

[3] C. Ortiz Dueñas, R.J. Miller, et al. Effect of length on compressor inter-stage duct performance[R]. ASME GT2007-27752, 2007.

[4] Zhang Guochen, Xu Zhihui, etc. Numerical study on the aerodynamic performance of a twin-ducted S-shaped duct. Journal of Shenyang Aerospace University, 2011, Vol.28 No.2 (In Chinese)

[5] Wang Yangang, Liu Bo, etc., The effect of the installation angle of the outlet support plate on the flow field distortion of the upstream stationary blade, Journal of Northwestern Polytechnical University, 2008, Vol.26 No.3 (In Chinese)

[6] Wang Yangang, Liu Bo, etc., Study on the Effect of the Circumferential Layout of Outlet Support Plates on the Upstream Flow Field, Propulsion Technology, 2006, Vol 27 No.3 (In Chinese)